




# Real-time Volume Editing on Low-power Virtual Reality Devices

Iordanis Evangelou<sup>1</sup><sup>a</sup>, Anastasios Gkaravelis<sup>1</sup><sup>b</sup> and Georgios Papaioannou<sup>1</sup><sup>c</sup>

<sup>1</sup>*Department of Informatics, Athens University of Economics and Business, Athens, Greece*  
{iordanise@aueb.gr, agkar@aueb.gr, gepap@aueb.gr}

**Keywords:** virtual reality, ray casting, volume graphics.

**Abstract:** The advent of consumer-grade, low-power, untethered virtual reality devices has spurred the creation of numerous applications, with important implications to training, socialisation, education and entertainment. However, such devices are typically based on modified mobile architectures and processing units, offering limited capabilities in terms of geometry and shading throughput, compared to their desktop counterparts. In this work we provide insights on how to implement two combined and particularly challenging tasks on such a platform, those of real-time volume editing and physically-based rendering. We implement and showcase our techniques in the context of a virtual sculpting edutainment application, intended for mass deployment at a virtual reality exhibition centre.

## 1 INTRODUCTION


Today, consumer virtual reality (VR) headsets offer unprecedented image clarity and movement freedom. Coupled with vision-assisted spatial tracking and natural, 6-DoF interaction, these untethered, standalone VR systems provide an incredibly immersive VR experience in a multitude of applications, ranging from VR games and social networking to training and simulation applications. Despite the fact that modern VR headsets are more than capable to display 3D content at the very demanding frame rates and latency required for comfortable immersive stereo, their low power consumption and reduced weight constraints limit the devices' capabilities in terms of geometry and shading throughput, when compared to their desktop counterparts. This means that high-fidelity graphics pipelines that rely on ray tracing, or intensive geometry processing methods cannot be implemented efficiently in the underlying architectures and limited hardware resources of typical untethered VR systems. In most cases, applications are limited to a few hundreds of textured and directly lit polygons and even forgo dynamic lighting in many cases, to keep rendering passes down to a minimum and pixel shaders simple. Going beyond the typical rendering tasks in such a setting, is quite challenging, not only due to the hardware limitations of standalone VR systems,


but also due to the necessary rigidity of typical game engines used for the application development.

In our case, we wanted to perform real-time editing of solid geometry and the respective display of the result using physically admissible shading. As explained next, such an application requires an intensive geometry processing stage and results in too many primitives for a low-power rendering platform to handle. This paper presents the methodological approach used to perform real-time volumetric editing and display, combining techniques such as multi-view voxelisation, image-domain ray marching and stochastic visibility checks. The resulting application, intended for mass deployment at a virtual reality exhibition centre, was developed in Unity with custom shaders and was able to run at 68 frames per second on an **Oculus Quest 2**.

### 1.1 The Target Application

The goal was to implement an immersive application, where a solid block of material could be carved and shaped in a fully dynamic and therefore unpredictable manner, to create a new form, like sculpting and clay modelling in the physical world (Figure 1). The user has access to a selection of electric rotary and impact tools with various drill bits as well as a "fill gun" that deposits modelling paste on the sculpture for additive editing and corrections. The tools can be exchanged by picking them up from a workbench near the model using one of the 6-DoF controllers. The removal or

<sup>a</sup> <https://orcid.org/0000-0003-4556-390X>

<sup>b</sup> <https://orcid.org/0000-0002-9673-2462>


<sup>c</sup> <https://orcid.org/0000-0003-4774-0746>



Figure 1: Screenshots from the virtual sculpting VR application.

deposition of material is performed by touching the drill bit or nozzle of the virtual tool onto the surface of the sculpture (Figure 1 - bottom).

The virtual sculpting application provides three sculpting modes: expert free-form modelling, constrained sculpting and creative mode. In the first mode, the user starts with a lump of rock, which must shape with the available tools. The second mode is the constrained sculpting mode, which is intended for novice users and enforces an indestructible solid boundary. In essence, the user "reveals" a predefined figure by chipping away material with the given tools. The third mode is the creative mode, where the process starts from an already sculpted shape, which the user can modify freely to personalise or transform it into something entirely different.

After a predetermined time, the user is signalled to stop editing and the resulting model is exported as a watertight polygonal model for 3D printing in STL format. The user is given a unique mnemonic visual identifier (badge) after the completion of the VR sculpting session that can be used for requesting the model to be sent via email or ordering the 3D printout of the model at a dedicated booth. The VR application packs and uploads the STL model on a dedicated

server for this task.

Apart from the typical technical requirements for high and stable framerate and responsiveness valid for all VR applications, the particular edutainment installation had to be able to run on standalone VR headsets for the following reasons. First, the application should be deployed in multiple devices simultaneously in a large space, in order to accommodate multiple visitors. Second the deployment should be cable-free for the safety of the visitors and the easy access of the exhibition personnel to assist the users. Finally, device redundancy, maintenance, replacement and sanitisation introduce logistic constraints on the size, weight and compactness of the chosen solution.

## 1.2 Technical Challenges

The implementation of the volume editing and rendering for the standalone VR system is especially challenging and required an innovative approach to volume editing and display, as explained in the following sections.

Solid modelling at such a fine-grained and unstructured manner can only be performed on volumetric representations, either single-level or hierarchical. To provide ground for enough detail on the sculpted figures, but also reduce discretisation artifacts during rendering at a typical working distance, a volume representation of no less than  $128^3$  voxels must be used.

At each frame, collision of the tool's active surface with the volume elements must be detected to both allow and block the tool from penetrating the boundary surface of the edited volume and mark the affected elements for modification. To allow inter-operation with the collision and event system of the game engine, this task must be performed on the CPU and take as little time as possible. Note that in the particular volume editing application, an additional geometry processing task must take place: that of volume island elimination. As the user progressively removes material from the solid model, at some point bits may end up levitating in the air, unsupported and disconnected from the main body of the model. These regions must be identified and their elements removed. This step can be performed by a graph-processing algorithm, which however is quite expensive, especially at the required volume resolution.

After all necessary changes are made to the volumetric representation, the modified boundary surface of the model must be rendered. Typically this entails one of two approaches: either conversion to triangular mesh and rasterisation using the pipeline provided by the game engine, or direct volume visualisation using ray marching. The first means that the vol-

ume must be triangulated, either globally or locally at the region of change, using a variant of the marching cubes algorithm (Lorensen and Cline, 1987). Although local updates are efficient, updating vertex and element buffers of variable length is not. Furthermore, the total number of triangles resulting from the volumetric model can be several hundred thousands, which renders this option inapplicable to untethered VR. Triangulation becomes even more problematic, since the triangulated meshes must be smoothed and vertex normals estimated in the updated regions and their boundaries.

On the other hand, direct volume rendering using ray marching can be performed in a more controllable manner, with the option to trade visual fidelity for speed in order to maintain the desired frame rate. However, it implies two things: first, the rendering pipeline of the game engine must be circumvented for the particular game object and second, the volume representation must be resident on GPU memory and constantly updated. The latter proved to be an especially heavy task in Unity, which does not provide access to texture subloading functionality. The custom rendering for the sculpted volume translates to implementing all shading with custom shaders. Furthermore, since the game engine is agnostic to the volumetric representation, interaction with light sources, including shadows, cannot use the rendering passes of the former. A positive side-effect of this is that custom lighting allows us to model more realistic light-volume interaction, more suitable for the often translucent materials used.

## 2 RELATED WORK

We present here a brief overview of prior art relevant to the tasks at hand in our application, i.e. geometry representation for dynamic updates and visualisation approaches for such data. We deem a review of the general volume editing and related VR applications out of the scope of our discussion, since we focus on the specific case of *untethered* VR, where prior art is scarce.

**Volumetric representations.** Since direct editing of geometric meshes with arbitrary operations can lead to heavy re-tessellation and topology changes, a triangulated mesh representation is typically avoided in digital sculpting applications. Even more so in our case, where the computing resources of an untethered VR system are limited. On the other hand, volumetric representations offer a generic and fast approach to represent arbitrary shapes, at a user-controlled precision. Volumetric data, expressing the presence of the

geometric shape at a given spatial partition, can easily be accomplished using a uniform grid representation (Lagae and Dutré, 2008), which is an inexpensive choice in terms of construction and update, but can become prohibitively expensive on storage requirements. Alternatively, resorting to image-based regular grids (Vardis et al., 2016; Karabassi et al., 1999) can be lighter to maintain and equally fast to update on every consecutive frame. Complexity of spatial queries is constant on both of these structures but can induce divergence if variable size lists of primitives are maintained for each voxel (for analytic computations), instead of being treated as discretised boolean volume presence (occupancy) indicators. To represent and process larger and more detailed geometric shapes, uniform grids can be hierarchically built. Hierarchical approaches include the popular Sparse voxel octree (Laine and Karras, 2010) and hierarchical irregular grids (Pérard-Gayot et al., 2017), but such methods are inapplicable to our case, since we not only need per-frame updates of the data structure, but there is also limited amount of memory bandwidth for data representation.

**Volume - ray intersection queries.** Depending on the voxel grid representation, ray traversal or *marching* within a volume towards a potential hit cell can be achieved either analytically (Amanatides and Woo, 1987), exhaustively evaluating all possible ray - cell hits along the footprint of a ray or, approximately using a digital differential analyzer (DDA) algorithm (McGuire and Mara, 2014). Both approaches can be adapted either for image-domain or world-space ray traversal and also account for hierarchical representations, as in the Quadtree Displacement Mapping image-space ray traversal (Drobot, 2010). In our work, to minimise thread divergence within fragment invocation, we employ a variant of the DDA algorithm with a constant number of samples, since the resolution of the volume is fixed, hence the worst case traversal length.

Signed distance fields (SDFs) (Bloomenthal and Wyvill, 1997) is another popular approach to quickly traverse empty space in ray marching and represent level sets of complex procedural shapes. A distance field is a spatial function that reports the minimum distance of a given point from the level set. The SDF replaces the absolute distance with a signed one, indicating the sidedness. This information can be used for safely skipping empty space while traversing a volume, whose occupancy boundary can be considered a discretised level set isosurface. It can also be used to iteratively compute intersections with the isosurface. We do not generate a full distance field for our model, which would be required for empty space skipping,

since the volume is constantly updated and SDF computation is rather expensive. However, we exploit a generic algorithm to identify the closest intersection point on the SDF, the sphere tracing (Hart, 1995), to better approximate a smooth shading point and normal from a ray marching hit point (see Section 4.2).

### 3 VOLUME EDITING

The application provides a range of tools to the user in order to perform two main tasks: a) carve and remove material from the sculpted mass and b) deposit new material over the edited geometry, to enable corrections in a plausible manner. Volumetric editing occurs at each application update iteration and at each update cycle, the selected tool interacts with the shell of the volumetric representation up to a small depth, using either a spherical or rectangular cutter/filler. These primitives are fast to analytically intersect with the volumetric cells, but other shapes can also be integrated, if required.

#### 3.1 Collision Detection

Collision detection with the elements of the discretised volume of fixed resolution can be done in linear time with respect to the intersected volume mass. To allow for the detection of arbitrary overlaps between the sculpted volume and the tool tip primitive, the cutter/filler primitive is transformed to the sculpture's local reference frame. The bounding volume of the transformed primitive is computed and discretized at the granularity of the sculpted volume, and each voxel of the transformed primitive bounding volume is checked for collision with the sculpted volume voxel state. We perform this linear pass over the volume samples on the CPU, since multiple updates must take place and feedback to the game logic has to be provided, before updating the GPU-side representation, such as tool transformation freeze for penetration avoidance and controller force feedback.

#### 3.2 Volume Representation

The representation of the solid's volume requires its content to be resident and updated in both the host and the device side to properly visualise it. Therefore, data transactions on every frame for a fixed binary grid (e.g.  $128^3$  in our case) can cause redundant, heavy updates and data transfer operations, since the user is only interacting with a small volume partition near the sculpt surface. Inspired from the depth-buffer-based voxelisation technique by (Karabassi

et al., 1999), to overcome this issue, instead of using a voxel array for the volumetric data representation, we model the binary grid using 3 two-dimensional arrays. The cells of these arrays store the minimum and maximum ranges of the occupied field along each dimension (see Figure 2 - left). The editing operations are then transformed from flipping the state of each binary voxel to, shrinking or widening the stored ranges accordingly (see Figure 2 - middle). This reduces update operation complexity and the memory requirements from cubic to quadratic with respect to the grid resolution.

Implementation-wise, the range maps are compacted in a single texture array, with one layer for each major axis. Min/max ranges are stored normalised with single-byte precision as a two-channel texture, as all intersection computations are performed in the local reference frame of a unit cube, representing the effective working volume. Using a single texture for both min/max values facilitates coherent texture access and checking of a ray marching step with a single texture fetch (see Section 4.1).

The only drawback of this image-based volumetric representation is that it cannot model every possible shape as it cannot represent internal cavities or empty space in general that is not visible to at least one axial projection. Due to the nature of the task at hand though, this is not an issue in our application, since all operations occur on the outer shell of the sculpted volume, which is always visible in the range maps.

#### 3.3 Volume Initialisation

The application operates in three different modes: a) free-form sculpting, starting from a roughly cut lump of material, b) constrained sculpting, initialised as in the first case and c) surface modification, where the user processes an already formed shape. These modes are presented to the user in an introductory screen, as shown in Figure 3. Depending on the mode, the volume is initialised by extracting the 3 axial range map pairs using an approach similar to the depth buffer projection of (Karabassi et al., 1999). For modes (a) and (b), a pre-modelled lump of stone is sampled and used as the starting shape, whereas for mode (c), an easy to modify figure is used. We deliberately chose a nondescript toy model for this operation, since we did not want the user to operate on and thus probably deface a well-known historical figure.

Range maps are computed by a conservative software triangle voxelisation on the CPU, i.e. switching on *all* voxels intersected by the triangles, followed by voxel projection on the range maps. This is available

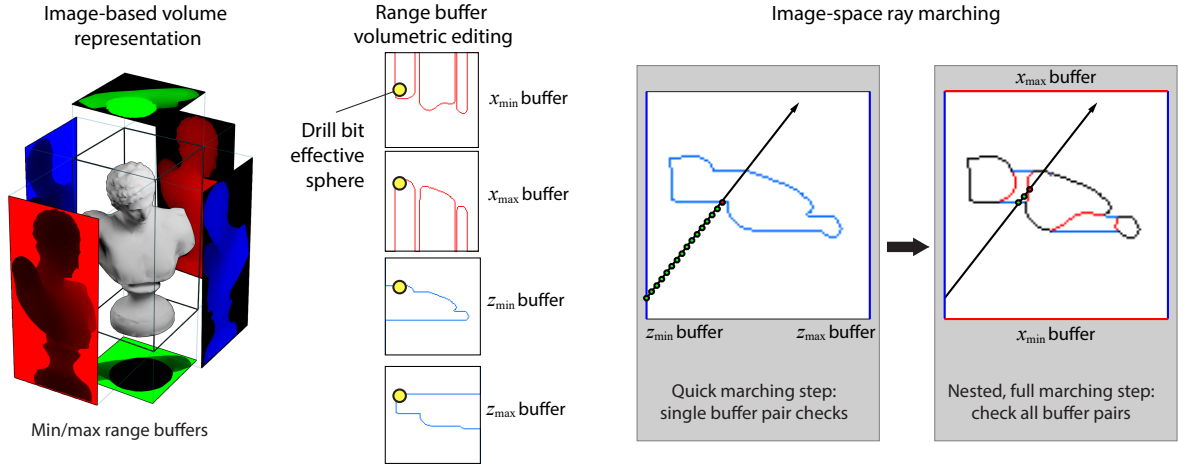


Figure 2: Image-based volume representation, editing and rendering via image-domain ray marching.

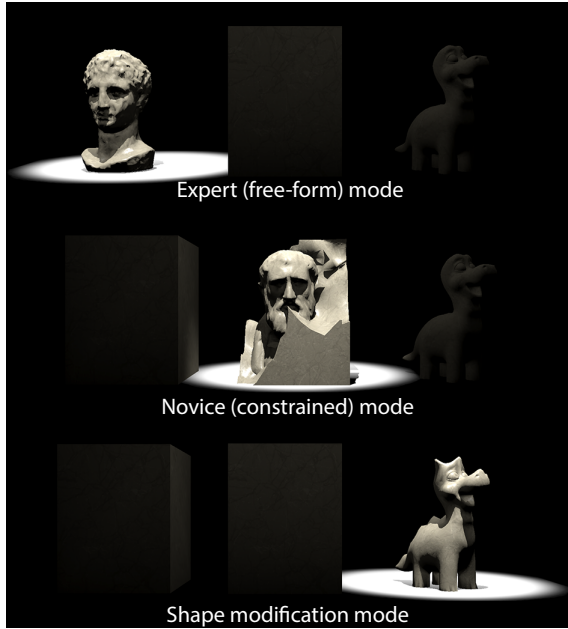


Figure 3: The three editing modes.

as a Unity pre-processing plugin from within the editor. The initial range maps need not be recomputed every time the application is initialised, so they are saved as assets and packaged along with the rest of the content.

### 3.4 Disconnected Part Elimination

As mentioned in Section 1.2, the application must be able to recognise at run time parts that are disconnected from the main body and are not supported from the ground and remove them. To handle this, we employ a flood fill algorithm, starting from the ground voxels and traversing the grid upwards. First, we

transform the range maps into a binary voxel grid and then traverse the volume. Voxels that were not visited during this process should be removed, by trivially updating the range values at the corresponding range maps. We update the contents of the original range maps by traversing the valid intervals of each coordinate and setting the new ranges based on the minimum and maximum voxel coordinates marked as *visited*.

We employ two additional modifications on this step to maintain interactive frame rates at run time. First, we assume that valid voxels appear only around the 6-neighbourhood of the pivot voxel (axis-aligned neighbours), instead of visiting all 26 adjacent voxels. This is a natural simplification in our case, since exclusively diagonal connections would imply an unstable structure anyway. Second, we amortise the execution of this operation over multiple frames by exploiting the *coroutine* programming pattern. This is achieved through splitting the flood fill loop and distributing the task over multiple consecutive frames until the sculpting volume has been completely processed. We have experimentally set the coroutine to *yield* at 100K flood fill iterations, that results in a good balance between smooth runtime experience and prompt removal of excess material.

### 3.5 Constrained Sculpting

In the constrained sculpting mode, which is intended for novice users and children, a target shape is hidden within the initial lump of material. The user gradually removes material to reveal the intended form within. To implement such a function, certain voxels should be specially marked as irremovable, so that any editing operation refrains from altering their state



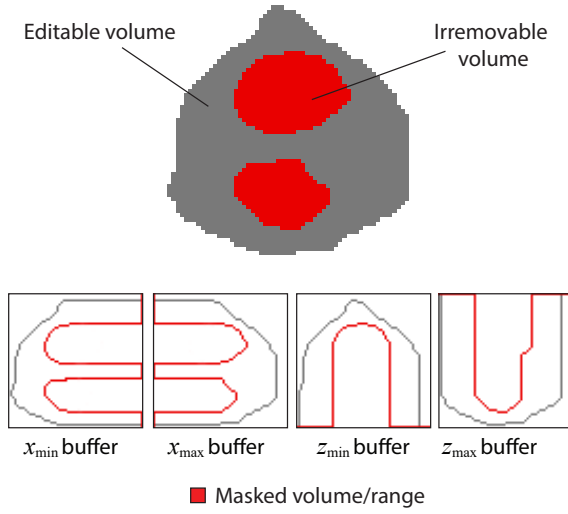


Figure 4: Volumetric masking for constrained sculpting. Additional range maps signify the axial ranges, where voxels cannot be modified.

(see Figure 4). In our image-based volume representation, this simply translates to using an additional set of range maps, which comprise the masked volume and are checked prior to modifying the intervals in the primary range maps for a particular voxel projection. The masking mechanism was straightforward to integrate within the volume editing step at an insignificant processing cost.

### 3.6 Geometry Export

The volume editing in our application case results in a tangible output. Although we have no noteworthy contribution to this stage, we present it here for completeness. When the editing session is concluded, the image-based volumetric information is converted to a mesh via an implementation of the Marching Cubes method (Lorensen and Cline, 1987). The resulting mesh is further smoothed out by applying two iterations of a Laplacian smoothing kernel of one-voxel radius at the neighbourhood of each vertex (Sorkine, 2005), and uploaded to a remote server in STL format for offline 3D printing. The particular filter size removes discretisation artifacts but retains geometric feature details.

## 4 VOLUME RENDERING

During rendering, the sculpted object is rasterised using the standard primitive shape of a unit cube, transformed to take up the intended size and final positioning in space. However, we replace the standard game

engine’s forward pass fragment shader with a custom one to perform all ray marching and lighting computations.

### 4.1 Ray Marching

As is typical in all modern rasterisation-based ray marching applications, starting from the interpolated object-space position of the (unit) cube at any given fragment in the fragment shader, we form a ray traversing the volume of the bounding cube inwards. However, in our case, ray traversal occurs in the image domain of the range maps, in a similar manner to screen-space ray tracing (McGuire and Mara, 2014). Normally, to evaluate each ray marching step, the occupancy (or density) of the voxel corresponding to the ray sample would be checked and the ray traversal terminated at a point between the occluded and unoccluded step. In our case, for each ray step this check would normally pertain to three texture fetches and a range check with the min/max values stored in the corresponding buffer cells on each major axis projection. However, we take advantage of the axial separation of the projected geometry to efficiently and conservatively traverse empty space with a single fetch at each ray step. Instead of continually checking all three range buffer pairs, we only perform the ray traversal on the range map corresponding to the axis most parallel to the user’s view direction (quick marching step in Figure 2 - right). If a ray hit is detected, only then we proceed to a second, nested ray marching loop that checks the remaining two axial range map pairs for intersection (full marching step in Figure 2 - right). Practically, this means that the inner ray marching loop will run for a very few ray steps, which correspond to either the single final hit (a hit must be confirmed by all axial range maps) or partially occluded positions in at least one range map. The ray marching terminates either when the ray sample is enclosed by all three range queries or when the ray exits the unit cube, in which case the fragment is discarded.

In terms of fragment shader implementation, since conservative traversal in the current VR hardware can induce unnecessary divergence due to the dimension size, we opt for a fixed number of regular steps (128 in our case). The two-step ray traversal strategy described above omits redundant memory accesses and improves memory access coherence.

### 4.2 Surface Normals Estimation

The solid volume should be presented to the user as a smooth surface, agnostic to the underline representa-

tion. Using a simple localised estimator for the normal vector at the ray intersection point (e.g. assuming cubical voxels) would invariably result in an unnatural, blocky appearance and the resulting image would be plagued by screen-space aliasing similar to the effect of texture minification. We attempt to address both issues by introducing a low-overhead approximation of the local surface around the voxel hit point. Specifically, we extract the occupied voxels in the 6-neighbourhood around the hit point for which we assume that they are represented by a blob implicit surface of radius equal to half the voxel size. Then we trace a ray offseted by half the voxel size backwards along the original ray direction, and report the closest hit  $\mathbf{x}_{shading}$  on the signed distance field (SDF) composed by the smooth union of these voxels. Evaluating the normal vector at that location typically requires the computation of the SDF value on the local neighbourhood. Since this operation can be costly on the current hardware, we replace it with the linear combination of the direction vectors from each occupied voxel  $\mathbf{v}_i$  in the 6-neighbourhood towards the evaluated intersection point  $\mathbf{x}_{shading}$ , weighted by their inverse square distance (Shepard, 1968):

$$\mathbf{n} = \text{normalize} \left( \sum_{i=1}^6 \delta_i \frac{\mathbf{x}_{shading} - \mathbf{v}_i}{\|\mathbf{x}_{shading} - \mathbf{v}_i\|^2} \right) \quad (1)$$

where  $\delta_i$  is an indicator function with value 1 if the voxel  $i$  is occupied and 0, otherwise.

### 4.3 Shadows and Surface Shading

With the ray intersection point and the normal estimated, the surface shading can take place. To neutralise the look of the sculpted surface, we assume a Lambertian material with a procedural marble texture using Perlin noise (Perlin, 1985) precomputed and stored in a 3D texture buffer.

Due to the constantly updated geometry of the sculpted volume and the changing orientation of the subject (the sculpture can be rotated on the stool for easier access), direct illumination and visibility must be evaluated in real time, per fragment. However, since we completely dispense with the regular forward shading computations due to ray marching, we cannot rely directly on any part of the game engine’s computed values, such as the shadow map(s). Therefore, for the computation of light source visibility for the direct lighting, we perform a hybrid visibility computation. First, for each shaded point, we do an extra ray marching iteration, albeit with a small number of steps (10 in our case) towards the directional light of the scene. The ray marching terminates at

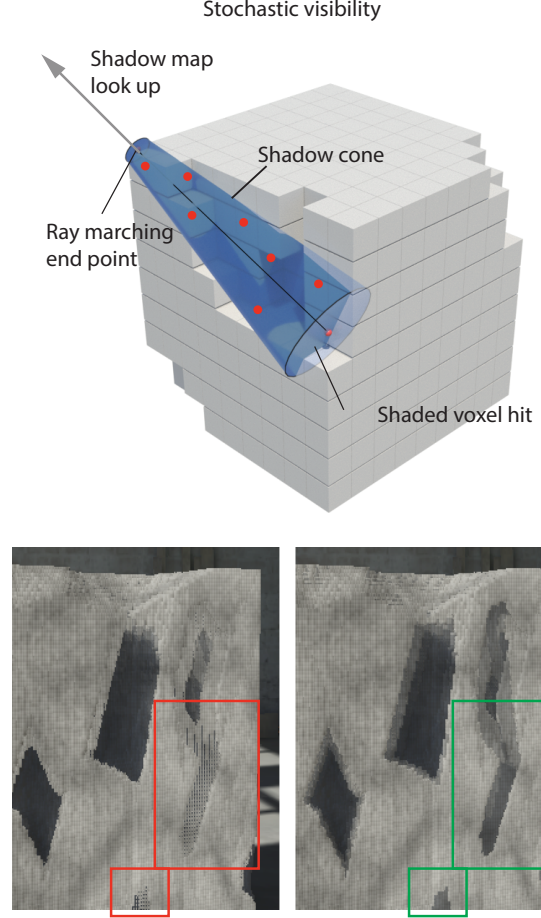


Figure 5: Visibility determination for volumetric shadows. Top: ray marching sample dispersion and visibility voting to account for subsurface scattering. Bottom: The effect of cone sample dispersion on shadow artifacts at oblique angles. Highlighted areas show aliasing artifacts (bottom-left) and how they are remedied (bottom-right).

the surface of the bounding cube. There, the shadow map is invoked to determine the visibility for the rest of the interval between the bounding box surface and the emitter.

To account for the translucent appearance of typical sculpting materials, we modify the visibility estimation in two ways. First, instead of terminating the shadow rays early, we allow the visibility term to be a continuous parameter, corresponding to a piecewise constant absorption of the traversed material. We initialise visibility with a maximum value of 1 and dampen it by a constant factor (0.7 in our case) for each occupied sample encountered during the ray marching loop. This is similar to modelling an exponential decay of the visibility factor according to the portion of the volume blocking the queried surface from the light source. Second, we offset the ray

samples away from the ray line within a tapered cone whose apex corresponds to the farthest ray box intersection (see Figure 5 - top). This effectively introduces some shadow softening imitating subtle sub-surface scattering for voxels near the surface, while leaving voxels in deep recesses unaffected. It also helps suppress artifacts of the visibility transitions at the discretised geometry at very oblique lighting angles. The effect is demonstrated in Figure 5 - bottom. The two cone radii correspond to  $2\times$  and  $0.25\times$  the voxel side for the shaded point and the ray segment terminus, respectively.

Finally, the indirect illumination component is approximately reconstructed from the spherical harmonics interpolated from the static light probe group baked for the environment, as provided by the Unity API.

## 5 RESULTS

We evaluate the performance of our method on an Oculus Quest 2 VR headset. The application was developed with Unity 2021.2.8 using the Oculus Integration SDK 37.0. All performance measurement were captured using the Oculus Developer Hub companion software.

We ran tests of our system on two precomputed volumes (see Figure 6) to stress the shader invocations workloads and avoid trivial fragment evaluations as in the case of the initial, bound-covering sculpting volume (see Section 3.3). Since the VR headset is configured to operate at a consistent framerate of  $13.8ms$  per frame (72 frames per second), we report the evaluation metrics of our method relative to this target and averaged over different orientations of the models.

**Relative rendering step impact.** For the volume rendering (Section 4), both examples operate on average at a 93.5% of the optimal performance, running at  $14.7ms$  per frame (68 fps), which is an acceptable level for a smooth experience. Omitting the SDF evaluation as described in Section 4.2 and directly processing the local shading with the intersection normal found from the closest voxel hit, the performance is sustained at the maximum level, with negligible impact. We also confirmed that by retaining the ray marching mechanism and SDF evaluation but, completely omitting the local shading (Section 4.3), still maintains the maximum level of performance.

**Ray marching performance.** For the same experimental setup, we compared the performance of ray marching with the deferred full comparison of ray samples described in Section 4 with that of a full ray marching loop, without the differed evaluation of co-



Figure 6: Two precomputed volume exemplars rendered with our proposed method, which were used for performance evaluation and fine-tuning.

ordinates. In the second case, we have registered a performance degradation of up to 17% (60 fps). As a final experiment, we also attempted to double the grid resolution (see Section 4), to improve the granularity and visual quality of the volume surface. The image-based volume representation, due to the quadratic dependence on volume resolution, instead of cubic for spatial grids, does not render the increase prohibitive. The performance hit is however noticeable, being on average 31% (50 fps) for both example volumes. As a result, for the currently presented method and hardware specification, this resolution is marginally attainable, but not recommended in terms of user experience and comfort.

**Temporal amortisation of material removal.** Lastly, in Section 3.4, we proposed the use of coroutine-based execution for amortising the computational cost of removing volumetric parts that are disconnected from the main sculpt body. As it is a computationally heavy method, naively executing this step on every frame, results in a reduction of the overall performance on the application's main experience to  $76ms$  per frame (13 fps) on average for both models, which is prohibitive. Due to the high cost, performing the full volume cleanup at once, but at a slower rate, is also problematic, since it results in disturbing framerate stuttering.

## 6 CONCLUSION

In this work, we proposed the mechanics to allow volume editing and rendering, two very demanding and intertwined tasks to run in real-time on untethered VR hardware. We described the necessary modifications, based on a careful selection and adaptation of established computer graphics methods and ideas and evaluated them in the context of a fully-functional and mass-deployed virtual sculpting application.

The presented methodology is suitable for volume editing applications similar to ours (e.g. 3D mod-



elling). However, the generalised application of the image-based volume representation to volumes of arbitrary complexity, and especially when these should include internal cavities or very occluded parts, is challenging and requires a multi-layer approach to handle correctly (Vasilakis et al., 2020).

Finally, an interesting approach, which requires further research and experimentation, would be to completely replace the underlying data structure with a truncated Signed Distance Field evaluator and respective data structure, in the spirit of VDB (Museth, 2013), along with the appropriate operators for editing the volume. This could greatly enhance the visual quality, minimise aliasing problems introduced by the discretization of the edited volume and potentially allow for arbitrary surface interactions. However, such an approach would require careful optimisation, in order to strike a balance between image quality and acceptable performance for an untethered VR device.

## ACKNOWLEDGEMENTS

This work was funded by the Foundation of the Hellenic World, Greece. Many thanks to Dimitrios Christopoulos, for his constructive comments and thorough application testing.

## REFERENCES

- Amanatides, J. and Woo, A. (1987). A fast voxel traversal algorithm for ray tracing. *Proceedings of EuroGraphics*, 87.
- Bloomenthal, J. and Wyvill, B. (1997). *Introduction to Implicit Surfaces*. Morgan Kaufmann Publishers Inc., San Francisco, CA, USA.
- Drobot, M. (2010). Quadtree displacement mapping with height blending. In Engel, W., editor, *GPU Pro - Advanced Rendering Techniques*, pages 117–138. A K Peters / Taylor & Francis.
- Hart, J. (1995). Sphere tracing: A geometric method for the antialiased ray tracing of implicit surfaces. *The Visual Computer*, 12.
- Karabassi, E.-A., Papaioannou, G., and Theoharis, T. (1999). A fast depth-buffer-based voxelization algorithm. *Journal of Graphics Tools*, 4(4):5–10.
- Lagae, A. and Dutré, P. (2008). Compact, fast and robust grids for ray tracing. In *ACM SIGGRAPH 2008 Talks*, SIGGRAPH '08, New York, NY, USA. Association for Computing Machinery.
- Laine, S. and Karras, T. (2010). Efficient sparse voxel octrees. In *Proceedings of the 2010 ACM SIGGRAPH Symposium on Interactive 3D Graphics and Games*, I3D '10, page 55–63, New York, NY, USA. Association for Computing Machinery.
- Lorensen, W. E. and Cline, H. E. (1987). Marching cubes: A high resolution 3d surface construction algorithm. In *Proceedings of the 14th Annual Conference on Computer Graphics and Interactive Techniques*, SIGGRAPH '87, page 163–169, New York, NY, USA. Association for Computing Machinery.
- McGuire, M. and Mara, M. (2014). Efficient GPU screen-space ray tracing. *Journal of Computer Graphics Techniques (JCGT)*, 3(4):73–85.
- Museth, K. (2013). Vdb: High-resolution sparse volumes with dynamic topology. *ACM Trans. Graph.*, 32(3).
- Perlin, K. (1985). An image synthesizer. *SIGGRAPH Comput. Graph.*, 19(3):287–296.
- Pérard-Gayot, A., Kalojanov, J., and Slusallek, P. (2017). Gpu ray tracing using irregular grids. *Computer Graphics Forum*, 36(2):477–486.
- Shepard, D. (1968). A two-dimensional interpolation function for irregularly-spaced data. In *Proceedings of the 1968 23rd ACM National Conference*, ACM '68, page 517–524, New York, NY, USA. Association for Computing Machinery.
- Sorkine, O. (2005). Laplacian Mesh Processing. In Chrysanthou, Y. and Magnor, M., editors, *Eurographics 2005 - State of the Art Reports*. The Eurographics Association.
- Vardis, K., Vasilakis, A. A., and Papaioannou, G. (2016). A multiview and multilayer approach for interactive ray tracing. In *Proceedings of the 20th ACM SIGGRAPH Symposium on Interactive 3D Graphics and Games*, I3D '16, page 171–178, New York, NY, USA. Association for Computing Machinery.
- Vasilakis, A. A., Vardis, K., and Papaioannou, G. (2020). A survey of multifragment rendering. *Computer Graphics Forum*, 39(2):623–642.